Solution Structure Determination of the Heme Cavity in the E7 His → Val Cyano-Met Myoglobin Point Mutant Based on the ^{1}H NMR Detected Dipolar Field of the Iron: Evidence for Contraction of the Heme Pocket†

Krishnakumar Rajarathnam,‡ Jun Qin,‡ Gerd N. La Mar,*,‡ Mark L. Chiu,§ and Stephen G. Sligar§

Department of Chemistry, University of California, Davis, California 95616, and Department of Chemistry, Biochemistry, Physiology and Biophysics and The Beckman Institute for Advanced Science and Technology, University of Illinois, Urbana, Illinois 61801

Received December 31, 1992; Revised Manuscript Received March 23, 1993

ABSTRACT: The ^{1}H NMR spectrum of the cyanomet complex of the sperm whale His[E7]Val myoglobin (Mb) point mutant has been analyzed by 2D methods to yield the assignments for the active site residues, including the substituted Val E7. The dipolar shifted proximal residues are used to quantitatively locate the magnetic axes for the paramagnetic susceptibility tensor in the molecular framework. The orientation of the major axis, which correlates with the ligand tilt, is ~15° from the heme normal, as found in wild-type (WT) Mb, but is tilted in a direction rotated ~40° toward the heme γ-meso position with respect to WT and similar to that in the His[E7]Gly mutant [Rajarathnam, K., La Mar, G. N., Chiu, M., & Sligar, S. G. (1992) *J. Am. Chem. Soc. 114*, 9048–9058]. The altered direction of an unchanged tilt angle for the Fe^{+3}–CN unit is shown to be qualitatively consistent with earlier computations of the potential energy surface for MbCO [Kuriyan, J., Wilz, S., Karplus, M., & Petsko, G. A. (1986) *J. Mol. Biol. 192*, 133–154]. It is concluded that His E7 does not significantly contribute to the ligand tilt but strongly influences the direction of tilt. Deviations between observed and predicted dipolar shifts for the E-helix backbone protons and perturbed patterns of their respective nuclear Overhauser effect between the E-helix and the heme 1,8-methyls are separately analyzed for movement of the E-helix and agree on a translation of the E-helix of the order of 0.8 Å in a direction toward the iron. The discrepancy between observed and predicted dipolar shifts for Phe CD1 indicates a ~0.5-Å movement by the ring parallel to the heme and towards the E-helix. The E-helix and Phe CD1 movements are consistent with a contraction of the pocket to fill the space created by the His → Val substitution. The correlation between the observed dipolar shifts of the substituted Val E7 side chain and those calculated as a function of rotation of the residue with and without movement of the E-helix confirm the movement of the E-helix and allow a quantitative description of the Val orientation. It is concluded that the dipolar field of the paramagnetic susceptibility tensor provides an important quantitative constraint for defining the heme cavity structure in cyanomet complexes of distal point mutants of myoglobin and hemoglobin.

Myoglobin serves as a textbook example for the control of protein function by local structure (Stryer, 1988). The distal histidine (E7) is a highly conserved residue among the myoglobins (Mbs)[1] and hemoglobins (Hbs) and is thought to play a key role in all aspects of ligand binding. It has been argued that Mbs and Hbs have evolved to selectively bind O_2 (Figure 1B) in preference to CO (Figure 1A), and this selectivity has been attributed to the ability of the distal histidine to stabilize binding of O_2 by hydrogen bonding and destabilize binding of CO by tilting it from a linear position (i.e., Figure 1C,D) (Phillips, 1980; Collman et al., 1976). The ferric cyanide complex, Fe^{3+}–CN, is isosteric with Fe^{2+}–CO (Figure 1A) and hence can serve as a probe for steric influences on ligand tilt (Figure 1C,D). Moreover, since the polar Fe^{3+}–CN unit is a hydrogen-bond acceptor, it can additionally serve as a sensitive probe for the distal interactions considered crucial for effective binding of O_2 (Lecomte & La Mar, 1987; Qin et al., 1992a). Sperm whale (Springer & Sligar, 1987) and other mammalian Mbs (Varadarajan et al., 1985; Smerdon et al., 1991) have been expressed, and numerous point mutants have been produced which allow a more systematic evaluation of the structural constraints of distal residues than previously afforded by limited natural genetic variants.

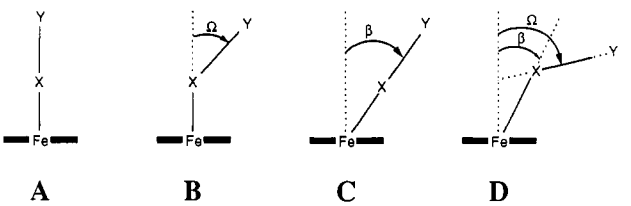

FIGURE 1: Binding modes of a diatomic ligand XY: (A) Linear and perpendicular to heme (like Fe^{2+}–CO and Fe^{3+}–CN in model heme compounds); (B) bent (like Fe^{2+}–O_2); (C) linear and tilted from heme normal by angle β, and (D) tilted (by β) and bent. The angle between the *XY* axis and the heme normal is ω.

The apparent steric destabilization of bound CO (or CN^-) in Mb and Hb is most directly observed in single-crystal

† This research was supported by Grants HL-16087 (G.N.L.), GM-33775 (S.G.S.), and GM-31756 (S.G.S.) from the National Institutes of Health.

* To whom the correspondence should be addressed.

‡ University of California.

§ University of Illinois.

[1] Abbreviations: NMR, nuclear magnetic resonance; WT, wild type; Mb, myoglobin; metMbCN, cyanomet myoglobin; NOE, nuclear Overhauser effect; metMbCN, ferric cyanomyoglobin; MbCO, carbonmonoxymyoglobin; XANES, X-ray absorption near edge; EXAFS, extended X-ray absorption fine structure; 2D, two dimensional; NOESY, two-dimensional nuclear Overhauser effect spectroscopy; COSY; two-dimensional bond correlation spectroscopy; MCOSY, magnitude COSY; TOCSY, two-dimensional total correlation spectroscopy; DSS, 2,2-dimethyl-2-silapentane-5-sulfonic acid; ppm, parts per million.

0006-2960/93/0432-5670$04.00/0

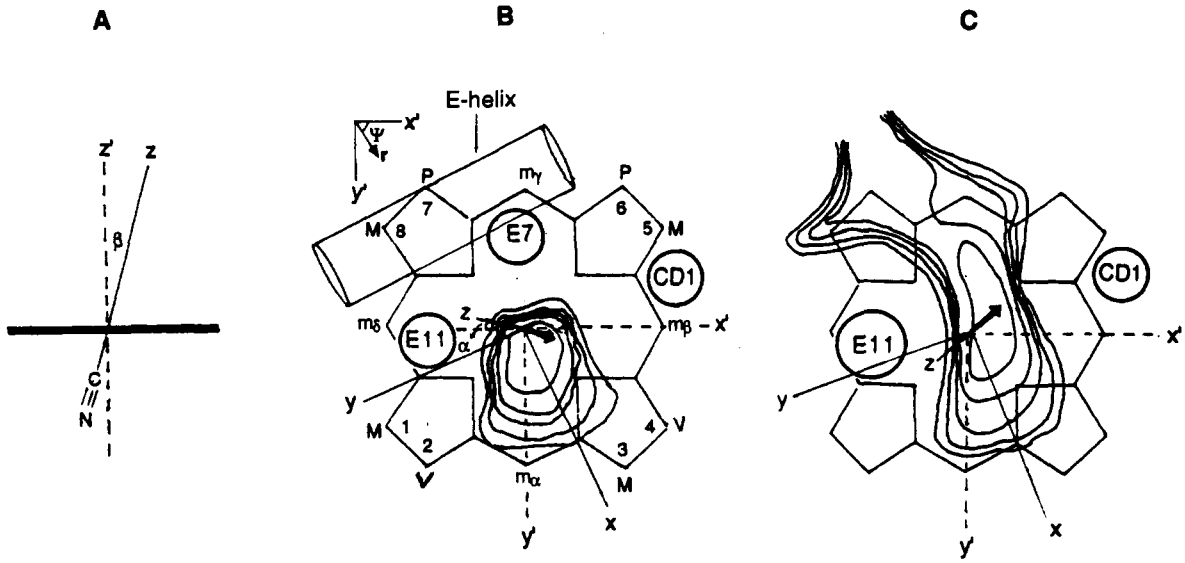

FIGURE 2: Orientation of magnetic axes, x,y,z, relative to heme symmetry axes, x',y',z'. (A) β is the tilt of the z axis from the heme normal, z'; (B and C) α is the angle between the projection of the z axis on the heme plane and the x' axis, and the in-plane or rhombic magnetic axes are related to x',y' by the angle $\kappa = \sim\alpha + \gamma$, where α,β,γ are the standard Euler angles that rotate x',y',z' into x,y,z. The heme pyrrole substituents are designated as M, P, and V for methyls, propionates, and vinyls respectively; the four meso positions are labeled m_α, m_β, m_γ, and m_δ to distinguish them from the use of α, β, and γ for the Euler angles. The lines in panel B represent the energy contour of an O atom of a bound CO (2.5 Å from the heme plane) due to van der Waals interaction with the nearby residues His E7, Val E11, and Phe CD1, adapted from Kuriyan et al. (1986). The solid arrow represents the point where our magnetic axes place the N atom from the bent but linear Fe^{3+}–CN unit, and this position corresponds reasonably to the potential energy minimum. The lines in panel C represent the energy contour for the same O atom with the E7 His rotated out of the pocket, as adapted from Kuriyan et al. (1986), which is a reasonable model for the His[E7]Val mutant. The minimum in the potential well is now a trough that extends toward the γ-meso position. The solid arrow indicates where the magnetic axes place the N atom at 3.0 Å, and the movement of the arrow point is along the trough toward the new minimum. The approximate position of the E-helix backbone is given in panel B, where the vector with length r and angle Ψ with respect to the x' axis on the heme is defined along which movements over the heme plane of the whole E-helix and Phe CD1 are considered.

diffraction studies where the oxygen (or nitrogen) is found well off the normal to the heme (Figure 1B–D) (Kuriyan et al., 1986; Steigemann & Weber, 1979; Derewenda et al., 1990; Deatherage et al., 1976). More recent neutron diffraction work has shown that the Fe–CO unit in sperm whale Mb is both tilted and bent (i.e., Figure 1D) (Cheng & Schoenborn, 1991). A variety of spectroscopic methods have been shown to be capable of monitoring aspects of this tilt/bend of the Fe–CO(N) unit, which include polarized infrared (Braustein et al., 1988; Moore et al., 1988), resonance Raman (Yu, 1986; Li & Spiro, 1988), XANES (Bianconi et al., 1985), EXAFS (Powers et al., 1984), and, more recently, ^{1}H NMR spectroscopy (Emerson & La Mar, 1990b; Rajarathnam et al., 1992). NMR is applicable only to the cyanide-bound ferric (metMb) form and relies on the determination of the orientation of the magnetic axes of the paramagnetic susceptibility tensor of this low-spin ($S = {}^1/_2$) ferric ion (Figure 2A,B). Detailed studies on wild-type (WT) metMbCN have shown that (1) the assignments of the heme pocket residues most strongly influenced by the paramagnetic dipolar field are readily attainable by 2D NMR methods (Emerson & La Mar, 1990a; Yu et al., 1990), (2) the resultant experimental dipolar shifts, together with the available crystal coordinates of the isostructural MbCO complex, allow quantitative determination not only of the orientation of the magnetic axes but also of the axial and rhombic magnetic anisotropies, and (3) the orientation of the magnetic axes and the magnitude of the anisotropies are accurately determined by experimental ^{1}H NMR data solely from the proximal residues which can be expected to be essentially unperturbed due to a single distal point mutation (Emerson & La Mar, 1990b; Rajarathnam et al., 1992). The resultant magnetic axes for WT metMbCN have the major magnetic axis, as expected to be determined by the Fe–CN bonding, tilted from the heme normal by $\sim$15° toward the β-meso position (Figure 2A,B), which is essentially collinear with the orientation of the Fe–C vector in the MbCO crystal as determined by neutron diffraction (Cheng & Schoenborn, 1991). X-ray crystal structures of the *Chironomus* monomeric HbCO and metHbCN reveal very similar distortion of the Fe^{2+}–CO and Fe^{3+}–CN units (Steigemann & Weber, 1979). It is thus clear that solution ^{1}H NMR spectroscopy of the cyanomet complex of Mbs and Hbs provides an alternate probe of distal heme pocket influences on ligand tilt. Compared to other spectroscopic methods, it has the advantage, like single-crystal studies, of providing both the *magnitude* as well as the *direction* of the tilt of the bound ligand.

^{1}H NMR spectroscopy has shown the hyperfine shifts of the metMbCN complex of a distal point mutant to be extremely sensitive to replacement of His E7 by Gly (Rajarathnam et al., 1992). Moreover, the proximal side heme pocket residues of His[E7]Gly metMbCN were shown to be essentially unperturbed by the distal point mutation. The experimental dipolar shifts of the proximal residues of the His[E7]Gly mutant yielded an orientation of the magnetic axes whose angles are as accurately determined as for the WT and whose magnetic anisotropies were minimally altered from those of the WT complex. Although the extent of the tilt of the major axis in the His[E7]Gly mutant was found to be very similar to that in WT metMbCN, the direction of the tilt was significantly changed. Before formulating a structural interpretative basis for the orientation of the magnetic axes in terms of distal influences on Fe–CN tilt, it is necessary to establish that the response in the NMR spectral parameters, and the resulting orientation of the magnetic axes, reflect a systematic perturbation in the distal pocket. To this end, we extend our ^{1}H NMR studies here to the His E7 → Val point mutant. The His[E7]Val, as well as the previously studied His[E7]Gly mutant, should reflect primarily the influence of the removal of the imidazole side chain on the magnetic axes

and hence the orientation of the bound ligand. Our goals are not only to determine the magnetic axes in His[E7]Val metMbCN and hence the orientation of the bound ligand but also to explore the prospects for using the experimentally determined magnetic dipolar field, in conjunction with conventional distance constraints, as a probe for establishing the nature of any general structural changes in the distal pocket that accompany the substitution of His E7 by Val.

MATERIALS AND METHODS

Sample Preparation. The His[E7]Val mutant was expressed and purified as previously described (Springer & Sligar, 1987). Cyanometmyoglobin (metMbCN) samples were exchanged with a solution containing 200 mM KCl and 20 mM KCN in ^2H_2O at pH 8.6 on an Amicon ultracentrifuge cell. ^1H_2O samples were made as described above with the exception that the solutions were in 90% ^1H_2O and 10% ^2H_2O so as to provide the lock signal.

^1H NMR Measurements. All the ^1H NMR spectra were collected on the GE Ω 500 and the NICOLET NT-500 spectrometers. The WEFT (Gupta, 1976) pulse sequence was used to produce spectra that suppress the slowly relaxing diamagnetic envelope and enhance the intensity of broad, rapidly relaxed signals. Nonselective T_1 values were obtained by the inversion–recovery experiment and are reproducible to ±10%. Steady-state NOEs were recorded as described in detail previously (Emerson & La Mar, 1990a); the ratio of NOEs to a common proton upon saturating two different heme methyl peaks was obtained from the ratio of the amplitudes of the NOEs in the difference traces. The magnitude COSY (Aue et al., 1976) (MCOSY) (n-type) spectra were collected at various temperatures from 10 to 45 °C in ^2H_2O over a spectral window of 10 000 Hz using 1024 t_2 complex points; 100–200 scans were collected for each block with a total of 400–512 t_1 blocks; the repetition time was 350 ms, and the total acquisition time is ~9 h. Phase-sensitive 2D NOE (NOESY) spectra (Jeener et al., 1979) were collected at 30 °C in ^2H_2O over a spectral window of 23 255 Hz using 1024 complex points in the t_2 dimension; 224 scans were collected for each of 256 t_1 increments. The mixing time used in this experiment was 50 ms. The repetition time was 350 ms, and the total acquisition time was ~12 h. The TOCSY spectra at 30 and 40 °C were collected in ^2H_2O over a spectral window of 11 049 Hz using 1024 t_2 complex points. The spin lock, using the MLEV-17 mixing scheme (Bax & Davis, 1985), was for 30 ms and the trim pulse for 2 ms. A total of ~140 scans were collected for each of the 256 increments collected. The repetition rate was ~1.5 s/scan, and the total acquisition time was ~24 h. Quadrature detection along the t_1 dimension was achieved as described by States et al. (1982). The residual ^1H_2O signal was saturated using a decoupler pulse for 200–300 ms in the relaxation delay time. All 1D data were processed on a SPARC station using GE UNIX Ω software. All 2D data were processed on a Silicon Graphics workstation using the Felix program written by Dr. Dennis Hare, and the processing parameters are outlined in figure legends.

Magnetic Axes Determination. The magnetic axes were determined as described in detail previously (Emerson & La Mar, 1990b; Rajarathnam et al., 1992). Experimental dipolar shifts for the structurally conserved proximal side of the heme were used as input to search for the Euler rotation angles, $R(\alpha,\beta,\gamma)$, that transform the molecular pseudosymmetry coordinates, x',y',z' or γ,θ',Ω' (Figure 2), (readily obtained from crystal coordinates) into magnetic axes, x,y,z, by minimizing the following error function:

$$F/n = \sum^{n} |\delta_{dip}(\text{obs}) - \delta_{dip}(\text{calc})F(\alpha,\beta,\gamma)|^2 \quad (1)$$

where

$$\delta_{dip}(\text{calc}) = -\frac{1}{3N}\left[\Delta\chi_{ax}(3\cos^2\theta' - 1)r^{-3} + \frac{3}{2}\Delta\chi_{rh}\sin\theta'\cos 2\Omega' r^{-3}\right] \quad (2)$$

and

$$\delta_{dip}(\text{obs}) = \delta_{DSS} - \delta_{dia} \quad (3)$$

$\Delta\chi_{ax}$ and $\Delta\chi_{rh}$ are axial rhombic anisotropies. δ_{dia} is the shift in the isostructural diamagnetic MbCO complex (Dalvit & Wright, 1987; Chiu, 1992) or calculated for protons whose δ_{dia} are not available by using the equation (Qin et al., 1992b)

$$\delta_{dia} = \delta_{sec} + \delta_{rc}, \quad (4)$$

where δ_{sec} is the shift of an amino acid proton typical for α-helices, β-strand, coils, etc. (Wishart et al., 1991), and δ_{rc} is the heme-induced ring current shift of the proton based on the WT coordinates by using the eight-loop model (Cross & Wright, 1985). Minimizing the error function F/n in eq 1 was performed over three parameters, α,β,γ, using available $\Delta\chi_{ax}$ and $\Delta\chi_{rh}$, or extended to all five parameters to yield both the Euler angles and anisotropies (Rajarathnam et al., 1992).

Dipolar Shift Simulations. The dipolar shifts for structural elements expected to be perturbed in the point mutant relative to WT (i.e., distal side) were analyzed to gauge the nature of the perturbations. For a perturbed proton, δ_{dip}(calc) from eq 2 based on WT coordinates usually deviates significantly from δ_{dip}(obs) in eq 3. In such a case, not only was δ_{dip}(calc) recalculated on the basis of the altered proton coordinates but δ_{dip}(obs) from eq 3 was corrected relative to that based on WT coordinates since δ_{dia} for an altered proton position is different from that based on WT coordinates. δ_{dia} for the altered proton was obtained from eq 4 by calculating the δ_{rc} term on the basis of the altered proton coordinates relative to WT coordinates.

RESULTS

Resonance Assignments. The resolved regions of the 500-MHz ^1H NMR spectrum of His[E7]Val metMbCN in ^2H_2O, pH 8.6, at 25 °C is illustrated in Figure 3A. A nonselective spin–lattice relaxation rate determination provides the T_1 values for resolved hyperfine-shifted protons as listed in Table I. The super-WEFT ^1H NMR trace at 25 °C, collected under rapidly pulsing conditions that emphasize broad, strongly relaxed resonances, is shown in Figure 3B. Two strongly relaxed ($T_1 < 4$ ms) and extremely broad signals (~400 Hz) are characteristic of F8 His (93) ring protons (Emerson & La Mar, 1990a; Qin & La Mar, 1992). The general appearance of the resolved portions of the ^1H NMR trace is very similar to that of the His[E7]Gly metMbCN, and the assignment strategy developed for that mutant (Rajarathnam et al., 1992), as well as the WT complex (Emerson & La Mar, 1990b), was used here. The uniqueness of both scalar and dipolar connectivities is confirmed by the strong temperature dependence of the hyperfine-shifted resonances, as illustrated by the comparison of the 25 °C trace in Figure 3A and the 5 °C trace in Figure 3C. The heme and proximal side residues Leu F4(89), Ala F5(90), His F8(93), His FG3(97), Ile FG5(99), and Phe H15(138) exhibit COSY and intra- and interresidue NOESY cross peak patterns essentially identical to those in WT and His[E7]Gly metMbCN considered in great detail previously (Emerson & La Mar, 1990a; Yu et al., 1990;

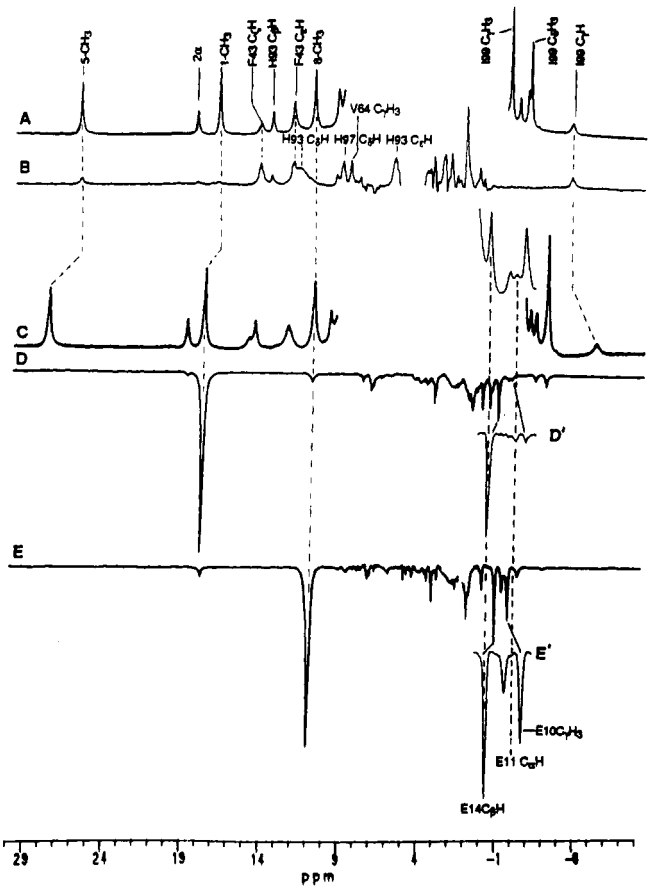

FIGURE 3: Resolved portions of the 500-MHz ^{1}H NMR spectrum of His[E7]Val metMbCN in ^2H_2O, pH 8.6, collected with a pulse repetition rate of (A) 1 s^{-1} at 25 °C and (B) 15 s^{-1} at 25 °C to emphasize the broad and fast relaxing lines, and (C) 1 s^{-1} at 5 °C where the E11 $C_\alpha H$ and E14 $C_\beta H_3$ signals are best resolved (see inset C'). Key resolved resonances are labeled as assigned in the text. Traces D and E are steady-state NOE difference traces upon saturating to the same degree (~90%) the heme 1-CH_3 and 8-CH_3 signals, respectively, at 5 °C. The insets D' and E' are the expanded portions of traces D and E showing the NOEs to E14 $C_\beta H_3$ and E11 $C_\alpha H$. Note the relative magnitudes to the signals assigned to Val E11 $C_\alpha H$ and E14 $C_\beta H_3$. The NOEs to E10 $C_\gamma H_3$ are also labeled in traces D' and E'.

Rajarathnam et al., 1992). Relevant 2D spectra with labeled cross peaks are shown in Supplementary Material, where the heme chemical shifts are also listed. Only NMR data relevant to defining the properties of distal residues, in particular, the substituted Val E7, are considered here in detail.

Signals from the six conserved distal residues of interest [Phe CD1(43), Phe CD4(46), Phe B14(33), Thr E10(67), Ala E14(71) and Val E11(68)] are readily identified. The combination of COSY cross peaks (Figure 4) and the characteristic short T_1 ~20 ms for $C_\zeta H$ (Figure 3B) and NOESY cross peak from Phe CD1 $C_\delta Hs$ to 5-CH_3 (Figure 5) identify the ring of PheCD1(43) with an orientation similar to that of WT. NOESY cross peaks (Figure 5) and 1D NOEs from Phe CD1 ring protons (not shown) to signals in the aromatic region exhibit among themselves two sets of COSY peaks which identify the weakly paramagnetically perturbed aromatic ring protons from Phe CD4(46) and B14(33) (not shown). Strong NOESY cross peaks from both 1-CH_3 and 8-CH_3 to a partially resolved upfield methyl (Figure 5), together with a single COSY cross peak to that methyl (Figure 4), identify Ala E14(71). A second upfield resolved methyl peak exhibits a strong NOESY cross peak to 8-CH_3 (Figure 5) characteristic of $C_\gamma H_3$ of Thr E10(67), and a COSY as well as relayed TOCSY peaks (Figure 4) locate the $C_\beta H$ and $C_\alpha H$. The NOESY data (Figure 5), as well as variable temperature 1D NOE experiments (shown at 5 °C in Figure 3D,E), identify a strongly upfield hyperfine-shifted single proton peak with T_1 ~ 100 ms with a relatively strong dipolar contact to 1-CH_3 and weak contact to 8-CH_3 which is identified

Table I: Chemical Shifts for Heme Pocket Amino Acid Residues in His[E7]Val metMbCN Mutants

resonance	δ_{obs}[a] (T_1)[b]	His[E7]Gly[e]	WT[e]
Phe B14/33			
$C_\delta Hs$	7.62	7.68	7.96
$C_\epsilon Hs$	7.82	7.91	8.31
$C_\zeta H$	8.39	8.89	8.31
Phe CD1/43			
$C_\delta Hs$	8.53	8.57	8.65
$C_\epsilon Hs$	11.89 (40)	12.26	12.39
$C_\zeta H$	14.06 (19)	13.12	16.93
Phe CD4/46			
$C_\delta Hs$	7.65	7.92	7.64
$C_\epsilon Hs$	7.50	7.50	7.98
$C_\zeta H$	7.96	7.66	7.64
Val E7/64			
$C_\alpha H$	5.68		
$C_\beta H$	4.84		
$C_{\gamma 1}H_3$	7.99 (~75)[c]		
$C_{\gamma 2}H_3$	3.29		
Thr E10/67			
$C_\alpha H$	3.00	3.05	2.50
$C_\beta H$	4.50	4.71	2.68
$C_\gamma H_3$	−1.32 (195)	−1.23	−1.49
Val E11/68			
$C_\alpha H$	−0.76 (~100)	−0.26	−2.36
$C_\beta H$	5.28	5.28	1.44
$C_{\gamma 1}H_3$	1.60	1.27	−0.97
$C_{\gamma 2}H_3$	*d*	1.79	−0.81
Ala E14/71			
$C_\alpha H$	3.49	3.49	3.48
$C_\beta H_3$	0.43	−0.28	−0.09
Leu F4/89			
$C_\alpha H$	7.46	7.36	8.53
$C_\beta H$	3.41	3.33	3.82
$C_\beta H'$	4.25	4.10	4.44
$C_\gamma H$	5.20	5.16	5.87
$C_{\delta 1}H_3$	3.41	3.15	3.93
$C_{\delta 2}H_3$	2.81	2.69	3.25
Ala F5/90			
$C_\alpha H$	6.74	6.64	6.40
$C_\beta H_3$	2.75	2.73	2.63
His F8/93			
$N_\rho H$	13.68		13.73
$C_\alpha H$	8.15	8.09	7.43
$C_\beta H$	13.11 (58)	12.88	11.40
$C_\beta H'$	9.01	8.80	6.34
$C_\delta H$	11.2 (~3)[c]	10.90	−4.30
$C_\epsilon H$	5.0 (~3)[c]	4.5 ± 2.5	18.80
$N_\delta H$	19.26		21.00
His FG3/97			
$C_\delta H$	8.6 (~20)	8.82	10.79
$C_\epsilon H$	5.97	6.17	6.84
Ile FG5/99			
$C_\alpha H$	2.98	3.14	2.38
$C_\beta H$	1.92	1.91	−0.09
$C_\gamma H$	−5.83 (70)	−5.36	−9.23
$C_\gamma H'$	−0.13	0.06	−1.78
$C_\gamma H_3$	−1.92 (180)	−1.83	−3.34
$C_\delta H_3$	−3.15 (167)	−2.90	−3.70
Phe H15/138			
$C_\delta Hs$	7.11	7.10	7.02
$C_\epsilon Hs$	7.25	7.22	6.94
$C_\zeta H$	7.66	7.55	7.05

[a] Chemical shifts in ppm referenced to DSS, in ^2H_2O at 30 °C, pH 8.6. [b] T_1 is given in parentheses, in milliseconds, as determined by nonselective inversion–recovery experiments (uncertainty ±10%) and calculated from null point, τ_{null} ($T_1 = \tau_{null}/\ln 2$). [c] T_1s are estimated from the super-WEFT experiment. [d] Not detected. [e] Taken from Rajarathnam et al. (1992).

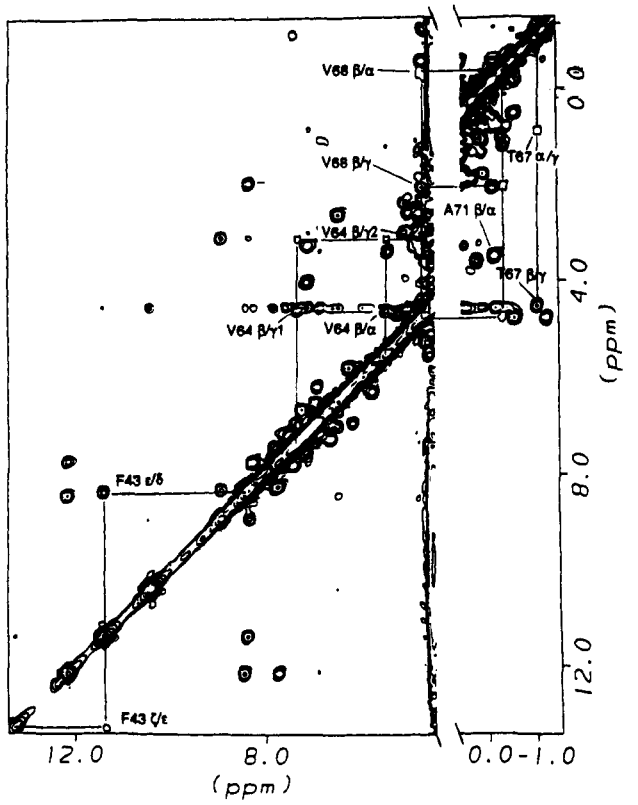

FIGURE 4: Portion of the 500-MHz ^{1}H MCOSY spectrum of the His[E7]Val metMbCN in ^2H_2O at 45 °C showing the spin connectivity patterns for the key distal residues Phe CD1(43), Val E7(64), Thr E10(67), Val E11(68) (in part), and Ala E14(71). The position of observed TOCSY cross peak is marked by square boxes. The spectrum was processed by applying an exponential decay function (2-Hz line broadening) and an unshifted sine-bell-squared window function over 256 points along both the t_2 and t_1 dimensions and zero-filling to 2K × 2K points.

as the Val E11(68) $C_\alpha H$. COSY peaks (Figure 4) identify the $C_\beta H$ and one of the $C_\gamma H_3$; the COSY cross peak needed to identify the other $C_\gamma H_3$ is not observed. This cross peak was weak in WT metMbCN due to the paramagnetic line broadening and is likely even broader in this mutant. The substituted E7 Val protons are located on the basis of two NOESY cross peaks from Phe CD1(43) $C_\epsilon Hs$ (Figure 5), which are observed in neither WT nor His[E7]Gly metMbCN (Emerson & La Mar, 1990a; Rajarathnam et al., 1992). These two resonances, one of which exhibits a strong temperature dependence, are shown by COSY and TOCSY data (Figure 4) to arise from a Val spin system, which must be due to E7 Val and is confirmed by the expected NOESY cross peak from the $C_\alpha H$ to the Thr E10(67) $C_\gamma H_3$ (not shown). One of the Val E7 methyl peaks at 8.29 ppm is best-resolved at 25 °C and exhibits a $T_1 \sim 75 \pm 20$ ms (i.e., $R_{Fe} \sim 5.8$ Å). Saturation of the Phe CD1 $C_\epsilon H$ signal leads to a ~–6% steady-state NOE to this E7 Val methyl peak (not shown), which translates[2] to an internuclear distance of ~3.4 Å.

Steady-state NOEs upon saturating 1-CH_3 and 8-CH_3 provide a more quantitative comparison[3] than the NOESY cross peak intensities of the relative distances of the Val E11(68) $C_\alpha H$ and Ala E14(71) $C_\beta H_3$ to the heme methyls, as illustrated in Figure 3D,E. The ratio of steady-state NOEs

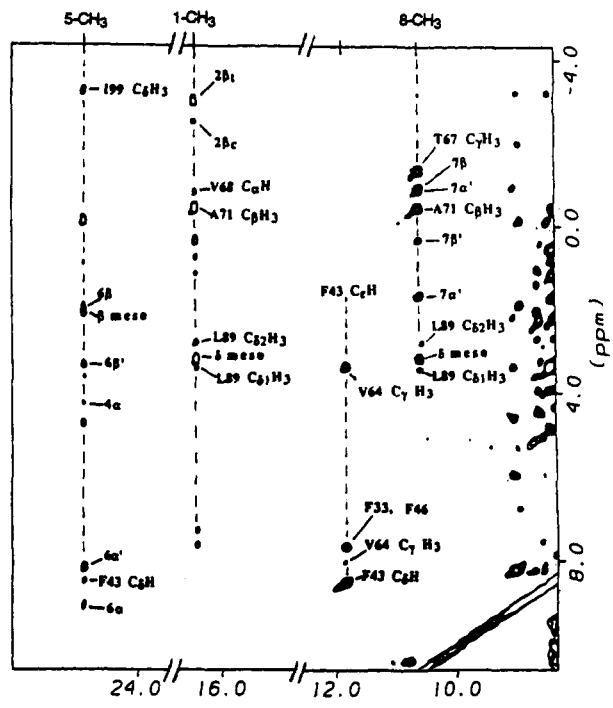

FIGURE 5: Low-field portions of the 500-MHz NOESY spectrum of the His[E7]Val metMbCN in ^2H_2O at 30 °C showing dipolar connectivities between the heme and key distal residues. Cross peaks of importance are labeled and are discussed in the text. The spectrum was processed by applying an exponential decay function and a 30°-shifted sine-bell-squared window function over 512 points along t_2 and 256 points along t_1 dimension and zero-filling to 2K × 2K points.

is defined as Q. For Ala E14(71) $C_\beta H_3$,

$$Q(\text{E14}) = \eta(\text{1-CH}_3 \rightarrow \text{E14 C}_\beta\text{H}_3)/\eta(\text{8-CH}_3 \rightarrow \text{E14 C}_\beta\text{H}_3) = 0.71 \pm 0.07 \quad (5)$$

in this mutant. This ratio of the NOEs in WT metMbCN is 0.50 ± 0.05 (Emerson & La Mar, 1990a), which agrees well with that predicted from the WT crystal structure [i.e., Q(E14) = 0.52]. For Val E11(68) $C_\alpha H$,

$$Q(\text{E11}) = \eta(\text{1-CH}_3 \rightarrow \text{E11 C}_\alpha\text{H})/\eta(\text{8-CH}_3 \rightarrow \text{E11 C}_\alpha\text{H}) = 3.0 \pm 0.5 \quad (6)$$

but Q is closer to ~1 in WT metMbCN (Emerson & La Mar, 1990a) in agreement with WT crystal coordinates. The Q values for the E7 Gly mutant are intermediate between those of WT and the present E7 Val mutant, but closer to the latter (not shown).

Determination of Magnetic Axes. We assume that the coordinates, and hence δ_{dia}, for proximal side residues in His-[E7]Val metMbCN are the same as those of the WT MbCO protein [see Rajarathnam et al. (1992) for details of the basis, justification, and experimental support]. No assumption is made as to whether the distal residue coordinates and/or δ_{dia} are conserved in the mutant (see below). The magnetic axes were determined by three-parameter least-squares searches for $R(\alpha,\beta,\gamma)$, using the experimental dipolar shift for two sets of resonances [14 and 9 proximal side peaks)[4] considered essential and sufficient [see Rajarathnam et al. (1992)]]. The magnetic anisotropies used are those determined by ^{1}H NMR for WT metMbCN using all 37 available shifts in a five-

[2] Steady-state NOE, $\eta(i \rightarrow j) = \sigma_{ij}T_{1j}$, where $\sigma_{ij} = -0.1\gamma^2h/^4r_{ij}^{-6}\tau_c$ and τ_c for a 17-kDa protein is estimated as 9 ns.

[3] Since steady-state NOE $\eta(i \rightarrow j) = \sigma_{ij}T_{1j}$, comparison of two NOEs to the same proton j eliminates the dependence of T_{1j}, i.e., $\eta(i \rightarrow j)/\eta(k \rightarrow j) = \sigma_{ij}/\sigma_{kj} = r^6_{kj}/r^6_{ij}$.

[4] The sets of proximal side resonances were defined as D′ (14 peaks; all six Ile FG5 signals, His FG3 $C_\delta H$, $C_\epsilon H$; Ala F5 $C_\alpha H$, $C_\beta H_3$; Leu F4 $C_\alpha H$; Phe H15 ring protons) and E (nine peaks; all six Ile FG5 signals, His FG3, $C_\epsilon H$, $C_\delta H$; Leu F4 $C_\alpha H$) in Rajarathnam et al. (1992).

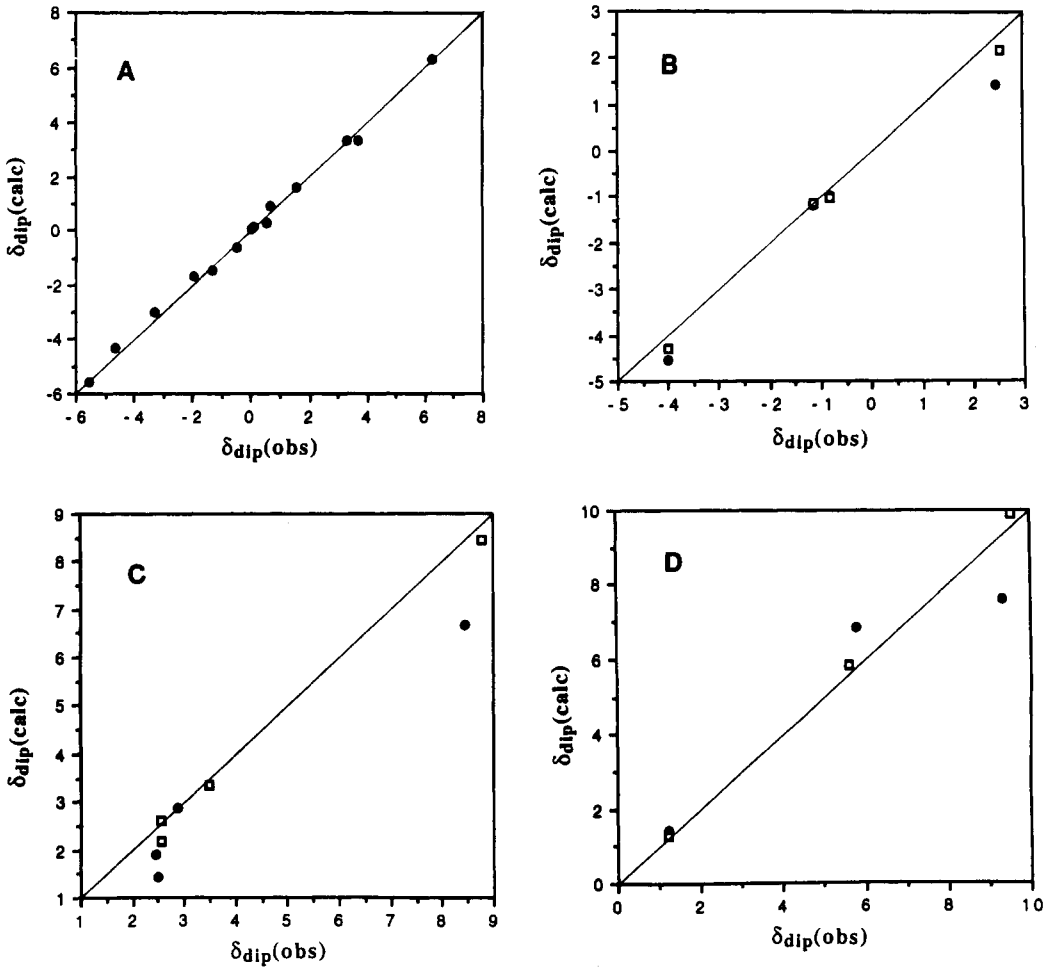

FIGURE 6: Plot of the observed versus calculated dipolar shifts for the magnetic axes $\alpha = -34°$, $\beta = 14.0°$, $\kappa (=\alpha + \gamma) = 73°$ and $\Delta\chi_{ax} = 1.12 \times 12^{-33}$ m^{-3}, $\Delta\chi_{rh} = 0.376 \times 10^{-33}$ m^{-3}. The solid line has unit slope and indicates a perfect fit. (A) Fourteen proximal residue signals used to determine the magnetic axes (closed circles); note the excellent fit by proximity to the line with unit slope. (B) C_αHs for the E-helix residues E7, E10, E11, and E14 based on WT position of E-helix (closed circles) (note the poor fit for some E-helix C_αHs to line with unit slope) and upon moving the E-helix 0.8 Å in a direction $\Psi \sim 80°$ (open squares). (C) Resonances for Val E7 upon minimizing F^*/n for the residue as a function of α–β bond rotation[7] for the WT E-helix (closed circles) and upon moving the E-helix 0.8 Å along the direction $\Psi = 80°$ (open squares). (D) Resonances of the aromatic ring of Phe CD1 for the orientation as in WT MbCO (closed circles) and upon minimizing F^*/n for the residue for the translation of the ring 0.5 Å along the heme surface in a direction $\Psi = -90°$ (open squares).

parameter search, $\Delta\chi_{ax} = 1.12 \times 10^{-33}$ m^{-3} and $\Delta\chi_{rh} = 0.376 \times 10^{-33}$ m^{-3} (Rajarathnam et al., 1992); the previously calculated anisotropies, $\Delta\chi_{ax} = 1.22 \times 10^{-33}$ m^{-3} and $\Delta\chi_{rh} = 0.476 \times 10^{-33}$ m^{-3}, were also considered (Horrocks & Greenberg, 1973). Lastly, the least-squares search is extended to five parameters to also obtain $\Delta\chi$s. The results from these searches are as follows. The three different three-parameter and the five-parameter searches yield highly clustered angles in very narrow ranges, i.e., $\alpha = 32 \pm 6$, $\beta = 14.5 \pm 0.5$, and $\kappa(\sim\alpha + \gamma) = 42 \pm 5$, with F/n values in the range 0.022–0.070. Moreover, the extension to five parameters results in only a small decrease in the error function, minimal changes ($\leq 1°$ in α, κ; 0° in β) in any of the angles, and an insignificant change in the anisotropies (change is 0.04 and 0.07×10^{-33} m^{-3} in $\Delta\chi_{ax}$ and $\Delta\chi_{rh}$, respectively). These angles are as well determined (as narrow a range) as for the WT and His[E7]-Gly mutant reported previously (Rajarathnam et al., 1992); the data on the three proteins for the same three data sets[5] are compared in Table II. The details of the individual least-squares searches for His[E7]Val metMbCN are given in the Supplementary Material. Comparison of the orientations of the magnetic axes in Table II reveals that they are indistinguishable for the His[E7]Val and His[E7]Gly mutants. However, the z-axis tilt (β) for the two mutants is similar to that in WT, while the direction of tilt (α) in the two E7 mutants is rotated by $42 \pm 8°$ in the direction of the γ-meso (Figure 2C) compared to that in WT (Figure 2B).

Table II: Comparison of the Orientation of the Magnetic Axes in WT and His[E7]Val, Gly metMbCN[a]

protein	β	α	$\kappa (\sim\alpha + \gamma)$	$\overline{F/n}^c$
WT[b]	15.5 ± 0.5	10 ± 2	35 ± 5	0.054
His[E7]Gly[b]	13.5 ± 0.5	−32 ± 3	45 ± 5	0.029
His[E7]Val	14.5 ± 0.5	−32 ± 6	42 ± 5	0.054

[a] Based on the range of each angle obtained with three- and five-parameter fits for the 14 and 9 proximal residue resonance sets C′, E defined in footnote 4 (Rajarathnam et al., 1992). [b] Taken from Rajarathnam et al. (1992). [c] Mean F/n over the three-parameter least-squares searches.

The quality of the least-squares fit is illustrated in Figure 6A where a plot of the observed versus the calculated δ_{dip} for the 14 shifts (data set D′)[4] used as input data in the three-parameter search places all 14 points on or very near (closed circle) to the line with unit slope. Figure 6B shows the same data for distal backbone C_αHs for E-helix residues E7, E10, E11, and E14 (based on the magnetic axes obtained in Figure

[5] Three parameter searches using proximal data 14 and 9 proton sets D′, E defined in footnote 4, and the five parameter search for data set D′.

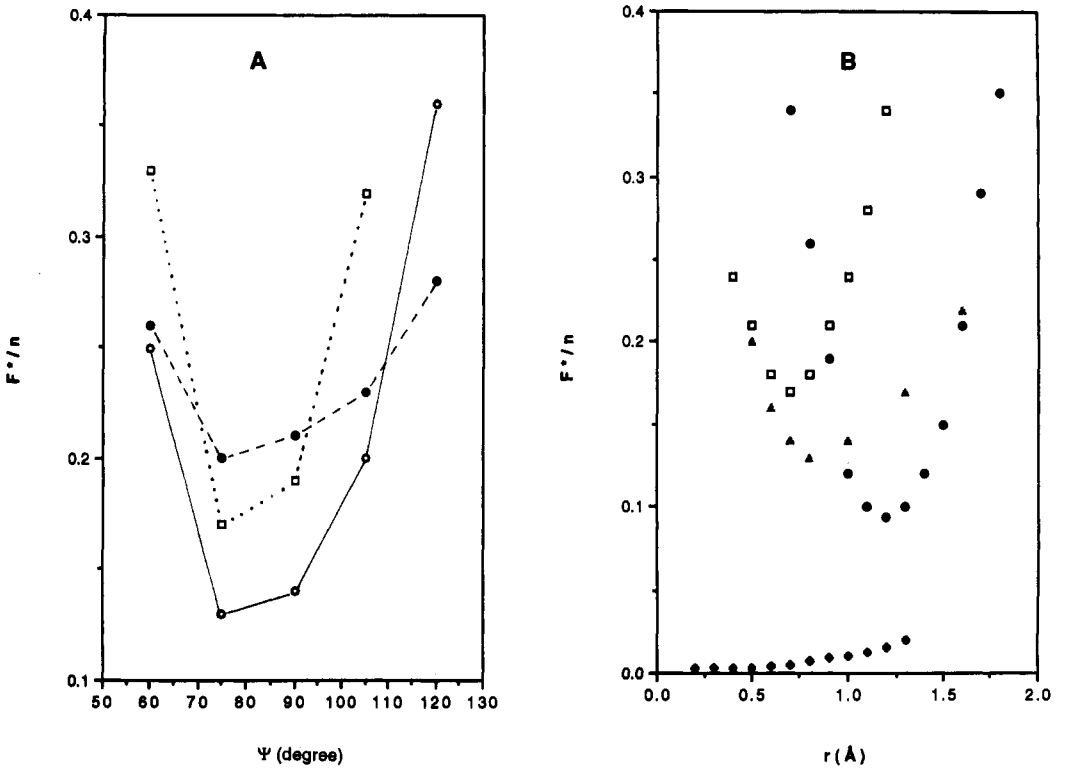

FIGURE 7: Plot of F^*/n' (A) as a function of the direction of movement, Ψ, for different magnitudes of the movement, r, for C_αHs of the three E-helix residues E7, E11, and E14 (E14, closed circles, 0.5 Å; E11, open circles, 0.8 Å; E7, open squares, 1.3 Å); note the minimum occurs at the same Ψ (80 ± 10°) for different r. (B) F^*/n' as a function of r for fixed Ψ ~ 80° (at the minimum in panel A) based on all four E-helix C_αH (closed triangles) and individual[8] C_αHs for residue E7 (closed circles), E11 (open squares), and E14 (closed diamonds). Note that the latter data suggest E14 C_αH moves less than E7 C_αH.

6A), some of which deviate significantly from the expected unit slope on the basis of an unperturbed E-helix position (closed circle). The plots of δ_{dip}(obs) vs δ_{dip}(calc) for the distal Phe CD1 ring protons based on the same magnetic axes are illustrated in Figures 6D (closed circle); the shifts exhibit significant deviations from the unit slope when compared to WT metMbCN (Emerson & La Mar, 1990b; Rajarathnam et al., 1992). For WT, magnetic axes determined solely from proximal side residues predicted the observed shifts for distal E-helix main chain and uniquely oriented side chain protons quite well (Rajarathnam et al., 1992). Hence deviations of δ_{dip}(obs) in the present mutant likely reflect structural differences, and a search for the perturbation(s), as supported by other distance (NOE) constraints, can elucidate the nature of the structural change. However, this requires that the structural change be unique and not represent an average over multiple structures. As discussed previously (Emerson & La Mar, 1990a), a reasonable criterion for this is that the variable temperature slopes of the chemical shifts be proportional to δ_{dip}(obs). This plot for the assigned resonance is shown in the Supplementary Material. The relationship is obeyed by all of the assigned resonances, except those for C_βH of Thr E10.[6]

Distal Structural Perturbations. This discrepancy between δ_{dip}(obs) and δ_{dip}(calc) based on the WT crystal coordinates can be used to define the nature of the likely structural changes. For this purpose we define a restricted error function for a limited set of protons of a particular residue, *R*:

$$R^*(R)/n' = \frac{1}{n'}[\delta_{dip}(\text{obs}) - \delta_{dip}(\text{calc})]^2 \qquad (7)$$

which is evaluated over the set of n' dipolar shifted protons influenced by the movement of *R*. An evaluation of F^*(E7 Val)$/n'$ for the four signals over the α–β rotational angle[7] ϕ based on the WT E7 C_α coordinates yields the plot in Figure 8A (closed circle), which yields a unique minimum with rather large F^*/n and whose optimal δ_{dip}(calc) show an improved, but still not an acceptable, fit to the straight line in the plot of δ_{dip}(obs) vs δ_{dip}(calc) in Figure 6C (closed circle). Moreover, for this fit, the shortest E7 Val methyl distance to the iron, R_{Fe}, is 6.3 Å, and that to the Phe CD1 C_ϵH is 3.9 Å, while the paramagnetic relaxivity indicates 5.8 Å and the steady-state NOE yield indicates 3.4 Å, respectively. Since Val E7 signals exhibit variable temperature slopes proportional to the δ_{dip}(calc) for the best fit (see Supplementary Material), the relatively poor fit of the E7 Val data to the available constraints suggests that the E-helix must be perturbed.

The assigned E-helix C_αH δ_{dip}(obs) values also deviate from δ_{dip}(calc) as shown in Figure 6B (closed circles). Since these protons are on the E-helix backbone, translation of the whole helix must be considered. We define a lateral movement of the whole helix over the heme by an amount r(Å) in a direction Ψ, as defined in Figure 2B. Initially, we assume r is the same for every E-helix backbone proton (i.e., the translated E-helix is parallel to the original E-helix). However, when r is not the same for each residue, the direction of movement, as defined

[6] The C_βH δ_{dip}(obs) shift of Thr E10 is found upfield from the δ_{dia} calculated for all orientations considered here, but the variable temperature slope is in the direction of larger δ_{dip}(obs) at higher temperature (i.e., opposite to that predicted by the Curie law; see Supplementary Material). Hence this side chain must exhibit multiple conformations [see Emerson and La Mar (1990b)].

[7] WT E7 His was replaced by Val E7 using the MIDAS program from the University of California, San Francisco. The HC_α–C_βH dihedral angle is defined as ϕ with ϕ = 0 for the eclipsed configuration. The rotation was made in a clockwise direction about C_α–C_β bond.

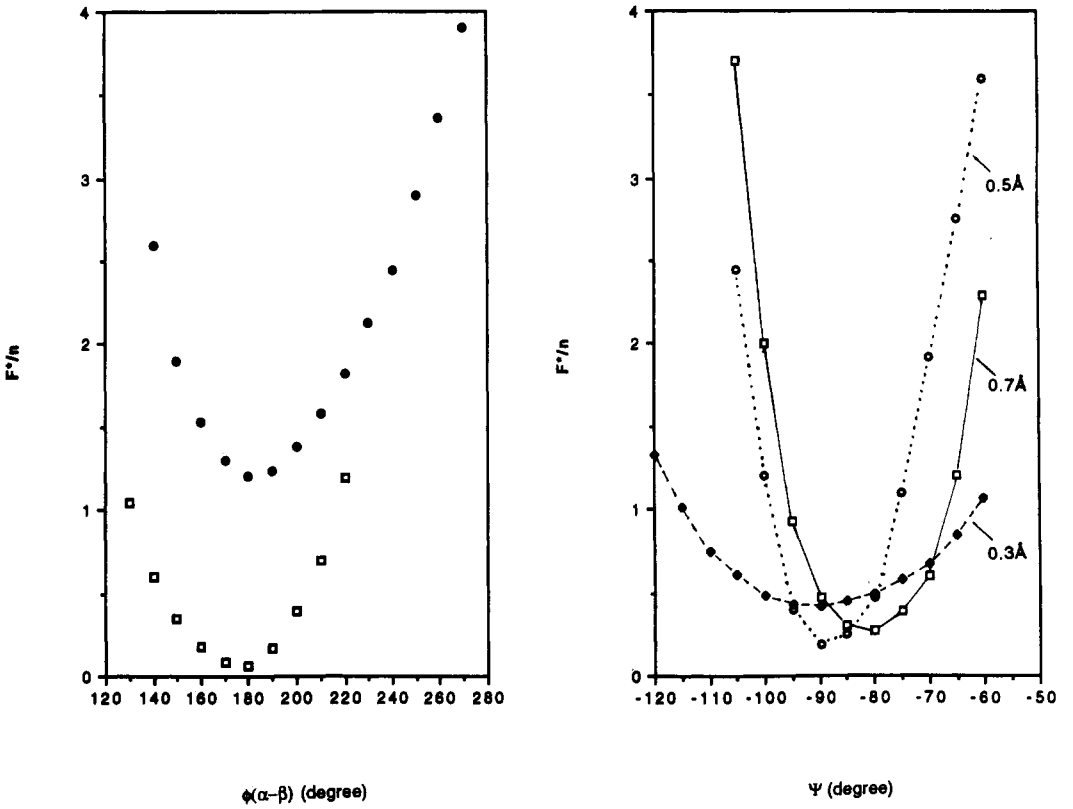

FIGURE 8: Plot of the error function, F^*/n, for a residue over the protons influenced by the movement described by (A) the Val E7 α–β bond rotation[7] for the E-helix as in WT Mb (closed circles) and for the E-helix moved 0.8 Å in the direction $\Psi = 80°$ (open squares) and (B) translation of the Phe CD1 parallel to the heme plane by **r** (Å) in a direction Ψ defined in Figure 2B,C (closed squares, 0.3 Å; open circles, 0.5 Å; open squares, 0.7 Å).

by Ψ, is still essentially the same for each residue.[8] Because of numerous van der Waals contacts between E-helix side chains and the heme, we do not consider E-helix movement perpendicular to the heme (see below). A plot of F^*(E-helix C_αHs)$/n'$ as a function of Ψ summed over the four residues E7, E10, E11, and E14, is shown in Figure 7A; a well-defined minimum is obtained with a significantly improved F^*/n over that for WT coordinates for $\Psi = 80 \pm 10°$ for all **r**. The plot of F^*/n over **r** for fixed optimal $\Psi \sim 80°$ is illustrated in Figure 7B (closed triangles). Again, a well-defined minimum is obtained for $r \sim 0.8 \pm 0.3$ Å. The δ_{dip}(calc) for the four E-helix C_αHs after ~0.8-Å movement in a direction $\Psi = 80$ provides a low F^*/n and significantly improved correlation with δ_{dip}(obs), as shown in Figure 6B (open squares). Hence the dipolar shifts for the E-helix backbone indicate a ~0.8-Å movement at $\Psi \sim 80°$.

A movement of the E-helix is directly supported by the altered steady-state NOE ratios from E11 C_αH, Q(E11) in eq 6, and from E14 $C_\beta H_3$, Q(E14) in eq 5, to the heme 1-CH_3 and 8-CH_3; both indicate the E-helix must have moved to bring it closer to 1-CH_3. An emphasis on lateral rather than vertical movement relative to the heme plane is directly dictated here, inasmuch as only the former will significantly alter the relative distances to the 1-CH_3 versus 8-CH_3 of an E-helix proton. The influence of the same movement of the whole E-helix by a variable **r** in a variable direction Ψ (Figure 2B) on the ratio of predicted NOEs,[3] as given by the Q values in eqs 5 and 6, is illustrated in Figure 9. The observed values of Q(E11) ~ 3 and Q(E14) = 0.7 are shown in this plot as boxes. The predicted ratio of NOEs is less restrictive on Ψ,**r** values than the F^*/n' in that a variety of combinations of **r**,Ψ are consistent with observed Q values (with Ψ restricted to be the same for both E11 and E14 C_αHs).[8] The need to account for increased Q(E11) and Q(E14) compared to WT ratios demands that movement be centered about $\Psi \sim 90°$ and be completely restricted to the range Ψ 30°–150° for $r \leq 1$ Å. Most importantly, the NOE data are consistent with $\Psi = 80$

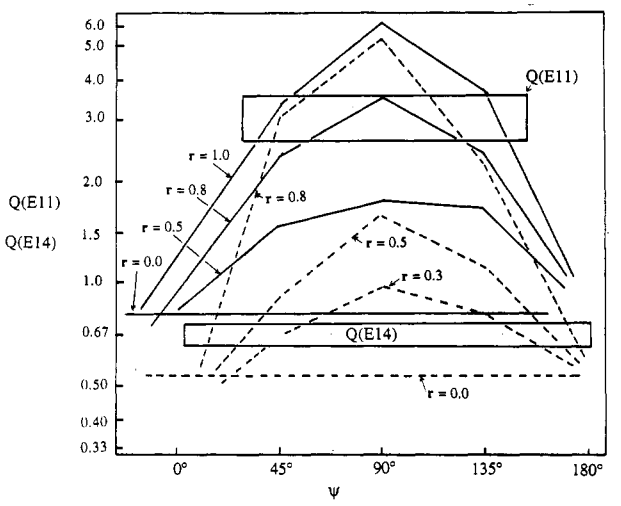

FIGURE 9: Plot of the steady-state NOE[3] ratios Q(E11) = η(1-CH_3→E11 C_αH)η(8-CH_3→E11 C_αH) (solid lines) and Q(E14) = η(1-CH_3→E14 $C_\beta H_3$)/η(1-CH_3→E14 $C_\beta H_3$) (dashed lines) as a function of the direction, given by the angle Ψ, and magnitude, given by **r**, of the lateral movement of the E-helix over the heme. The boxes reflect the uncertainties in Q(E11) and Q(E14) and show the region where the calculated values agree with experimental values.

[8] The calculation shows that if E7 C_αH moves by 1.3 Å in the direction Ψ ~80°, the angle for E14 C_αH to move by 0.5 Å is only ~78°. This is because the length of the E7–E14 helical segment is ~7.2 Å, which is much longer than the movement (~0.8 Å). Hence, the E7–E14 segment can be assumed to move in a common angle (i.e., 80°) even if E7 C_αH (~1.3 Å) moves more than the E14 C_αH (~0.4 Å).

± 10° and agree on a value of r in the range 0.4–0.8 Å. Larger r will restrict Ψ to values smaller or larger than 90° (Figure 9). It is noted that, while the NOE data agree on the direction and general magnitude of the translation of the E-helix, the data in Figure 9 indicate that, for any Ψ, the E11 $C_\alpha H$ must move farther than the E14 $C_\alpha H$ (see Discussion).

We now reconsider a search for the rotational position of Val E7 on the perturbed E-helix. The F^*(Val E7)/n' as a function of the α–β bond rotational angle,[7] ϕ, after moving the E helix 0.8 Å in a direction Ψ = 80°, is also included in Figure 8A (open squares). A clear minimum with excellent F^*/n' at ϕ = 180° is observed for which the correlation between δ_{dip}(calc) is as good as for the proximal side (Figure 8C, open squares). The quality of the fit is not significantly altered for r = 0.8–1.0 Å and for Ψ in the range 45–90° (not shown). Lastly, we consider the δ_{dip}(calc) for the only other residue for which all dipolar shifted signals are assigned; the shifts appear proportional to the variable temperature slope, but the δ_{dip}(obs) do not correlate well with δ_{dip}(calc) for the WT coordinates (Figure 6C), namely, Phe CD1(43). This totally invariant residue in Mb and Hb lies approximately parallel to, and in van der Waals contact with, the heme. For this residue, like the E-helix, only lateral movement over the heme plane is considered, where r is the magnitude of the translation and Ψ is the direction as described in Figure 2B. A plot of F^*(Phe CD1)/n for the ring proton signals as a function of both r,Ψ is shown in Figure 8B. A clear minimum is observed for r = 0.5 Å and Ψ ~ −90°, for which there is a significantly improved correlation between δ_{dip}(obs) and δ_{dip}(calc), as shown in Figure 6D (open squares).

DISCUSSION

Magnetic Axes Determination. The hyperfine shift pattern for heme pocket residues in His[E7]Val metMbCN is clearly different from that of WT (Emerson & La Mar, 1990a); moreover, this shift pattern differs from WT in essentially the same manner as previously found for His[E7]Gly metMbCN (Rajarathnam et al., 1992) (see Table I). The various proximal input data sets yielded magnetic axes with only small uncertainties in the Euler angles β, α, and κ ($\sim\alpha + \gamma$) of ±0.5, ±3°, and ±6°, respectively, as found previously for WT and the His[E7]Gly mutant, with similarly small error function, F/n = 0.03–0.07 (Rajarathnam et al., 1992). Hence, it is becoming clear that the assignment of dipolar shifted residues for the structurally conserved proximal residues, together with the crystal coordinates for these residues in a related derivative (such as sperm whale WT MbCO), provides an effective means to determine the magnetic axes of distal point mutant metMbCN complexes. Crystal coordinates for a number of other distal point mutants confirm the conserved proximal structure (Carver et al., 1992). The dipolar shifts for the assigned heme pocket residues for the His[E7]Val mutant translate to an orientation of the magnetic axes as defined in Figure 2C, with tilt of the major axes from the heme normal, β = 14.5 ± 0.5°, that is essentially the same as in WT (β = 15.5 ± 0.5), but with a projection on the heme plane, α = −32 ± 6°, that is rotated ~40° toward the α-meso position (Fe–CN rotated toward the γ-meso position) relative to WT (α = 10 ± 2°). The rhombic axes, as defined by $\kappa \sim \alpha + \gamma$ [which are much less sensitive to the NMR data; see Rajarathnam et al. (1992)], also remain similar to what is observed in WT and the His[E7]Gly mutant. Both the rhombic axes and the contact shift pattern reflect the nature of the orbital hole (Shulman et al., 1971; Palmer, 1978). The similar location of the rhombic axes is consistent with the largely unperturbed spin delocalization pattern in the heme. The magnetic axes for His[E7]Val metMbCN, moreover, are experimentally indistinguishable from those previously determined for His[E7]Gly metMbCN, as shown in Table II (Rajarathnam et al., 1992).

The Euler angles therefore detect a consistent response of the magnetic properties of the iron that represent largely the removal of the bulky imidazole side chain of the distal His. Essentially unaltered magnetic axes are obtained in three- and five-parameter searches confirming that the NMR data can determine anisotropies as well as orientation and that the magnetic anisotropies are inconsequentially altered in the mutant as found previously for His[E7]Gly (Rajarathnam et al., 1992). The conserved magnetic anisotropies, in spite of altered orientation of the axes, are consistent with the observation of only minor variations in the low-temperature g values for the lowest Kramers doublet for a number of distal point mutant metMbCN complexes (Chiu, 1992). It has been previously observed that, while the His F8 hyperfine shifts contain both contact and dipolar contributions, the changes in the observed shifts from those in WT upon introducing a distal point mutation are quantitatively accounted for by the change in dipolar shifts due to the reoriented axes (Rajarathnam et al., 1992). The His F8 ring shifts for the His[E7]Val are essentially identical to those of His[E7]Gly and quantitatively predicted by the change in magnetic axes from WT (Supplementary Material). This consistent and qualitative translation of the changed dipolar shift pattern of metMbCN point mutants into altered orientation of the magnetic axes strongly indicates that the magnetic axes can provide a quantitative interpretative basis for the NMR spectra not only for point mutants of sperm whale Mb but possibly also for natural genetic variants.

Relationship of Magnetic Axes to Ligand Tilt. The distortion of the linear Fe–CO(N) unit from the heme normal can take the form of a simple tilt (Figure 1C), a simple bend (Figure 1B), or both (Figure 1D). The various spectroscopic methods can reflect on one or the other (or both) of these distortions. In the case of the Fe^{3+}–CN unit, ligand field considerations of the magnetic properties of the metal ion dictate that the Fe–C bond, or the tilt of the Fe–C bond from the heme normal, would serve as the defining interaction for the major magnetic axis, inasmuch as it is the strongest bond in the complex (Palmer, 1978). Hence we conclude that the orientation of the major magnetic axis as determined by ^1H NMR in metMbCN reflects the extent of the Fe–C bond tilt from the heme normal, as defined by the angle β in Figures 1 and 2. The value of β = 15.5 ± 0.5° determined for WT (Emerson & La Mar, 1990a; Rajarathnam et al., 1992), is essentially the same as the tilt of the Fe–C vector from the heme normal (15°) as described by the neutron diffraction and X-ray studies of MbCO single crystal (Cheng & Schoenborn, 1991); moreover, the projection of the Fe–CO-(N) tilt is in the direction of the β-meso position in each case (Figure 2A,B).

The magnetic axes do not yield any information on whether the Fe^{3+}–CN unit is tilted (Figure 1C) or tilted and bent (Figure 1D). However, it has been proposed on the basis of XANES measurements on sperm whale metMbCN (Bianconi et al., 1985) and resonance Raman spectroscopy of *Chironomus* metHbCN (Yu et al., 1984) that the Fe^{3+}–CN unit is linear. The fact that the Fe–CO unit in MbCO (Cheng & Schoenborn, 1991) is bent and tilted could be the reason that the angle between the CO axis and heme normal (ω in Figure 1D), determined by polarized IR (Braunstein et al., 1988;

Moore et al., 1988), is larger (20–30°) than the tilt angle (β in Figure 1C,D) described herein. Whether the extents of tilt and/or bend of Fe^{2+}–CO and Fe^{3+}–CN are the same remains to be resolved. However, it is clear that the orientation of the magnetic axes of the metMbCN complex can serve as a valuable probe for exploring the relationship between distal pocket influences, as modulated by point mutations, and the extent and direction of the Fe–C tilt from the heme normal.

Distal Influences on Fe–CN/Magnetic Axes Tilt. The extent of the tilt of the Fe–C unit from the heme normal, β (as in Figure 1, panel C or D), in WT and His[E7]Val metMbCN [as well as His[E7]Gly metMbCN (Rajarathnam et al., 1992)] is found essentially unaltered at 14.5 ± 1.5°. The significant tilt/bend described by the C=O/heme normal angle in WT MbCO, as measured by polarized IR, is similarly undiminished in the His[E7]Gly MbCO mutant (Braunstein et al., 1988). Hence the imidazole ring of His E7 is clearly not responsible for the tilt. However, as shown by the present NMR data, the removal of the bulky imidazole ring in both the His[E7]Gly and His[E7]Val mutants changes the *direction* of the Fe–C tilt by ~40° toward the γ-meso position from that in WT (Figure 2C).

The relatively minor influence on tilt magnitude, but major effect on tilt direction of the bound ligand, finds rationalization in terms of the previously reported energy contour diagram computed for the oxygen atom of a bound CO as influenced by van der Waals interactions using the crystal coordinates of the distal residues (Kuriyan et al., 1986). The shape of the energy minimum with respect to the heme skeleton is reproduced in Figure 2B for the His E7 imidazole group in the heme pocket oriented toward the iron (WT) and with the E7 imidazole ring rotated so as to point out the heme pocket (Figure 2C). This latter situation can be considered as a good approximation of the "removal" of the imidazole ring in the case of His[E7]Val and His[E7]Gly mutant. The magnetic axes for WT metMbCN are given in Figure 2A, and the orientation of the major axis (–z axis, indicated by solid arrow with length of Fe–CN unit in Figure 2B) passes close to the potential energy minimum. The potential energy diagram indicates that the steep barrier against a linear and perpendicular Fe–CO is more likely the van der Waals interaction with Val E11 than with His E7. The orientation of the tilt, however, can be viewed as being determined by the van der Waals interactions with Phe CD1 and the His E7 imidazole ring. The change in the potential energy surface for the O atom upon rotating (removing) the E7 imidazole ring is to make the minimum shallower with a trough in the direction of the γ-meso position, as shown in Figure 2C. Also indicated in Figure 2C are the magnetic axes for the His[E7]Val (or His[E7]Gly) mutant (and the solid arrow for the Fe–CN unit), which show that the major axis has rotated in a manner to move to the new energy minimum resulting from the removal of the imidazole ring. This analysis leads us to conclude that His E7 should not be expected to strongly modulate the tilt/bend magnitude of the $Fe^{2+}CO/Fe^{3+}$ CN units but to strongly influence the direction of tilt. Moreover, it also suggests that it is the Val E11 that may serve as the major determinant of tilt magnitude. Preliminary ^{1}H NMR studies of E11 mutants in progress appears to confirm a key role for the E11 residue in modulating tilt (Rajarathnam, 1992).

Structural Perturbations in the Distal Pocket. The very similar NOESY patterns among proximal residues and between the proximal residues and the heme confirm an essentially unperturbed proximal side of the heme in the His[E7]Val mutant as compared to WT (Emerson & La Mar, 1990a). Moreover, the magnetic axes for the His[E7]Val (and His[E7]Gly) metMbCN mutants are as well-defined by the proximal residue coordinates and diamagnetic chemical shifts as in WT (Rajarathnam et al., 1992). For WT metMbCN, the magnetic axes determined solely on the basis of proximal side residues did an excellent job of predicting the observed distal residue δ_{dip}. For the present His[E7]Val, as for the His[E7]Gly mutant (Rajarathnam et al., 1992), however, the δ_{dip} for even backbone C_αHs are not well predicted. Also, simple rotation of the new introduced E7 Val failed to provide a good fit of the δ_{dip}, indicating that the E-helix position must be altered. Similarly, the change in the ratio of steady-state NOEs from the orientationally inflexible E11 C_αH and E14 $C_\beta H_3$ to the heme 1-CH_3 versus 8-CH_3 dictates a movement of the E-helix.

The direction and magnitude of the E-helix displacement deduced from optimizing the dipolar shifts, $\mathbf{r} \sim 0.8$ Å, $\Psi \sim 80°$, is qualitatively consistent with the observed alterations in the NOE pattern from E11 C_αH and E14 $C_\beta H_3$ to the heme. The significance of this displacement is underscored by the ability to obtain a qualitative fit to the substituted E7 Val shifts, and hence determine its orientation, for the relocated but not the WT E-helix. There are several other experimental constraints not explicitly considered in defining the movement of the E-helix and Phe CD1 or the orientation of the E7 Val. The closest approach to the iron of a Val E7 methyl allowed by the unperturbed E-helix is 6.3 Å, while the T_1 of $C_\gamma H_3 \sim 75 \pm 20$ ms dictates this distance as ~5.8 ± 0.2 Å. The proposed movement of the E-helix shortens this distance considerably, and the optimal E7 Val orientation on the moved E-helix yields a distance to the iron of 5.9 Å. Lastly, the closest approach between a Val E7 methyl and the closer Phe CD1 C_ϵH is reduced from 3.9 to 3.3 Å by these movements, which is consistent with the ~3.4-Å separation given by the NOE. In all cases, the structure determined solely on the basis of consideration of the dipolar field and E-helix → heme NOEs accounts for the other experimentally observed constraints. Hence we conclude not only that the dipolar shifts in low-spin ferric Mb and Hb allow the determination of the magnetic axes in distal point mutants but also that they can provide detailed information on the nature of both segmental and local structural changes that accompany the perturbation in the distal pocket.

The quality of the fits is surprising in view of the simplicity of the model considered, namely, only lateral movement of the whole E-helix. On the other hand, all supporting evidence considered above largely confirms the nature of the E-helix movement described. The translation of Phe CD1 ($\Psi \sim -90°$) is toward the E-helix (Figure 2B) and can be rationalized on the same basis as that for the E-helix, namely, the movement of nearby residues to fill the void over the iron resulting from the replacement of the bulky E7 His by the smaller Val side chain. Although the model for the E-helix movement is limited, the available data suggest refinements that could be confirmed once extensive sequence-specific assignments become available. For example, the NOE constraints in Figure 9 suggest that for any common angle,[8] Ψ, the E14 C_αHs moves less than E11 C_αH. Moreover, if F^*/n' for individual E-helix C_αHs are plotted as a function of $\mathbf{r}$ for the same (and optimized Ψ, as shown in Figure 8B, the optimal $\mathbf{r}$ value is 1.3 Å for E7 C_αH, 0.8 for E11 C_αH, and only 0.5 Å for E14 C_αH. Hence both constraints suggest that the E-helix has moved more at the beginning or center (i.e., E7) than near its terminus (i.e., E14). This is reasonable in that movement at the end of the E-helix is impeded by the tight E–F turn, and the invariance

of the F-helix would suggest that this turn is not perturbed. The beginning of the E-helix, however, is near the most variable and flexible portion of Mb and can be expected to move more readily (Case & Karplus, 1979; Kottalam & Case, 1988; Elber & Karplus, 1987).

All of the above data combine to provide compelling evidence that the substitution of His E7 by either Val (or Gly) leads to a small movement of the E-helix toward the heme iron in the solution structure of His[E7]Val metMbCN. The preliminary X-ray crystallographic data for His[E7]Gly MbCO also indicate a similar though smaller movement of the E-helix (G. N. Phillips, personal communication). The significant accommodation of the E-helix to the simple removal of the imidazole side chain, however, brings into question the interpretation of the tilt of the bound ligand based on the simple arguments presented above, inasmuch as the movement of the E-helix would shift the potential energy surface over the heme in Figure 2. The ready accommodation of the E-helix rather than the Fe^{3+}–CN tilt to the E7 substitution suggests that a more detailed interpretation of the factors influencing tilt be postponed until more structural information is available for both metMbCN and MbCO mutants. Several such ^1H NMR studies on metMbCN in this laboratory, as well as crystallographic studies on metMb and MbCO mutant complexes in other laboratories (G. N. Phillips, personal communication), are in progress. The present study, however, clearly indicates that ^1H NMR can serve as an important tool in defining the tilt of the Fe^{3+}–CN unit, and it will be of interest to compare the results on the modulation of ligand tilt of the Fe^{3+}–CN and Fe^{2+}–CO in the same mutants once such data become available.

ACKNOWLEDGMENT

The authors are indebted to K. Vyas for the measurement of the steady-state NOEs, to A. D. McPherson for assistance with computer programs, and to G. N. Phillips for the preliminary X-ray coordinates of His[E7]Gly MbCO.

SUPPLEMENTARY MATERIAL AVAILABLE

Three tables (chemical shift of heme, magnetic axes for various input data sets, and dipolar shifts for His F8) and three figures (variable temperature slope versus observed dipolar shift, upfield NOESY spectrum, upfield COSY spectrum) (5 pages). Ordering information is given on any current masthead page.

REFERENCES

Aue, W. P., Bartholdi, E., & Ernst, R. R. (1976) *J. Chem. Phys. 64*, 2229–2246.
Bax, A., & Davis, D. G. (1985) *J. Magn. Reson. 65*, 355–360.
Bianconi, A., Congiu-Castellano, A., Durham, P. J., Hasnain, S. S., & Phillips, S. (1985) *Nature 318*, 685–687.
Braunstein, D., Ansari, A., Berendzen, J., Cowen, B. R., Egeberg, K. D., Fraunfelder, H., Hong, M. K., Ormos, P., Sauke, T. B., Scholl, R., Schulte, A., Sligar, S. G., Springer, B. A., Steinbach, P. J., & Young, R. D. (1988) *Proc. Natl. Acad. Sci. U.S.A. 85*, 8497–8501.
Carver, T. E., Brantley, R. E., Singleton, E. W., Arduini, R. M., Quillin, M. L., Phillips, G. N., & Olson, J. S. (1992) *J. Biol. Chem. 267*, 14443–14450.
Case, D. A., & Karplus, M. (1979) *J. Mol. Biol. 132*, 343–368.
Cheng, X., & Schoenborn, B. P. (1991) *J. Mol. Biol. 220*, 381–399.
Chiu, M. (1992) Ph.D. Dissertation, University of Illinois, Urbana-Champaign, Urbana, IL.
Collman, J. P., Brauman, J. I., Halbert, T. R., & Suslick, K. (1976) *Proc. Natl. Acad. Sci. U.S.A. 73*, 3333–3337.
Cross, K. J., & Wright, P. E. (1985) *J. Magn. Reson. 64*, 220–231.
Dalvit, C., & Wright, P. E. (1987) *J. Mol. Biol. 194*, 313–327.
Deatherage, J. F., Loe, R. S., Anderson, C. M., & Moffat, K. (1976) *J. Mol. Biol. 104*, 687–706.
Derewenda, Z., Dodson, G., Emsley, P., Harris, D., Nagai, K., Perutz, M., & Renaud, J.-P. (1990) *J. Mol. Biol. 211*, 515–519.
Elber, R., & Karplus, M. (1987) *Science 235*, 318–321.
Emerson, S. D., & La Mar, G. N. (1990a) *Biochemistry 29*, 1545–1556.
Emerson, S. D., & La Mar, G. N. (1990b) *Biochemistry 29*, 1556–1566.
Gupta, R. K. (1976) *J. Magn. Reson. 24*, 461–465.
Horrocks, W. D., Jr., & Greenberg, E. S. (1973) *Biochim. Biophys. Acta 322*, 38–44.
Jeener, J., Meier, B. H., Bachmann, P., & Ernst, R. R. (1979) *J. Chem. Phys. 71*, 4546–4553.
Kottalam, J., & Case, D. A. (1988) *J. Am. Chem. Soc. 110*, 7690–7697.
Kuriyan, J., Wilz, S., Karplus, M., & Petsko, G. A. (1986) *J. Mol. Biol. 192*, 133–154.
Lecomte, J. T. J., & La Mar, G. N. (1987) *J. Am. Chem. Soc. 109*, 7219–7220.
Li, X.-Y., & Spiro, T. G. (1988) *J. Am. Chem. Soc. 110*, 6024–6033.
Moore, J. N., Hansen, P. A., & Hochstrasser, R. M. (1988) *Proc. Natl. Acad. Sci. U.S.A. 85*, 5062–5066.
Palmer, G. (1978) in *The Porphyrins* (Dolphin, D., Ed.) Vol. 4, pp 313–353, Academic Press, New York.
Phillips, S. E. V. (1980) *J. Mol. Biol. 142*, 531–554.
Powers, L., Sessler, J. L., Woolery, G. L., & Chance, B. (1984) *Biochemistry 23*, 5519–5523.
Qin, J., & La Mar, G. N. (1992) *J. Biomol. NMR, 2*, 597–618.
Qin, J., La Mar, G. N., Ascoli, F., Bolognesi, M., & Brunori, M. (1992a) *J. Mol. Biol. 224*, 981–987.
Qin, J., La Mar, G. N., Ascoli, F., & Brunori, M. (1992b) *J. Mol. Biol.* (submitted).
Rajarathnam, K. (1992) Ph.D. Dissertation, University of California, Davis, CA.
Rajarathnam, K., La Mar, G. N., Chiu, M., & Sligar, S. G. (1992) *J. Am. Chem. Soc. 114*, 9048–9058.
Shulman, R. G., Glarum, S. H., & Karplus, M. (1971) *J. Mol. Biol. 57*, 93–115.
Smerdon, S. J., Dodson, G. G., Wilkinson, A. J., Gibson, Q. H., Blackmore, R. S., Carver, T. E., & Olson, J. S. (1991) *Biochemistry 30*, 6252–6260.
Springer, B. A., & Sligar, S. G. (1987) *Proc. Natl. Acad. Sci. U.S.A. 84*, 8961–8965.
States, D. J., Haberkorn, R. A., & Reuben, D. J. (1982) *J. Magn. Reson. 48*, 286–292.
Steigemann, W., & Weber, E. (1979) *J. Mol. Biol. 127*, 309–338.
Stryer, L. (1988) *Biochemistry*, 3rd ed., W. H. Freeman and Co., New York.
Varadarajan, R., Szabo, A., & Boxer, S. G. (1985) *Proc. Natl. Acad. Sci. U.S.A. 82*, 5681–5684.
Wishart, D. S., Sykes, B. D., & Richards, F. M. (1991) *J. Mol. Biol. 222*, 311–333.
Yu, L. P., La Mar, G. N., & Rajarathnam, K. (1990) *J. Am. Chem. Soc. 112*, 9527–9534.
Yu, N.-T. (1986) *Methods Enzymol. 130*, 350–393.
Yu, N.-T., Benko, B., Kerr, E. A., & Gersonde, K. (1984) *Proc. Natl. Acad. Sci. U.S.A. 81*, 5106–5110.